
Data report: an electron backscatter diffraction study of a gabbroic shear zone, IODP Expedition 304/305¹

Angela Halfpenny² and David Prior²

Chapter contents

Abstract	1
Introduction	1
Methods and materials	2
Results	2
Acknowledgments	3
References	3
Figures	5
Table	10

Abstract

Integrated Ocean Drilling Program Expedition 304/305 was designed to investigate the formation and evolution of oceanic core complexes by drilling through the Atlantis Massif oceanic core complex. Characterization of shear zone microstructures from the Atlantis Massif provides information about the area's deformation history and insight into the formation of oceanic core complexes. Plastic deformation was recognized in only 3% of the recovered core volume. The majority of the shear zones are located in gabbroic lithologies. Using orientation contrast imaging and electron backscatter diffraction, petrofabrics and microstructures were compared between the center and the edge of a gabbroic shear zone collected from IODP Hole U1309D. Analysis of the crystallographic preferred orientation, internal deformation, and grain size variations of feldspar was also performed.

Introduction

Oceanic core complexes (OCCs) are domal bathymetric highs and have been recognized along ultraslow to intermediate spreading ridges (e.g., Cannat et al., 2006; Ohara et al., 2007; Okino et al., 2004; Smith et al., 2006; Tucholke et al., 1998). OCCs expose gabbroic rocks on the seafloor through detachment faulting and are often associated with serpentized peridotite.

The Atlantis Massif OCC is located at 30°N latitude on the Mid-Atlantic Ridge (MAR). The Atlantis Massif formed within the last 1.5–2 m.y. (Blackman et al., 1998, 2002). During Integrated Ocean Drilling Program (IODP) Expedition 304/305, a combined total of 1415.5 m was drilled through the footwall of the central dome of the Atlantis Massif OCC at Site U1309 (see the “[Expedition 304/305 summary](#)” chapter; Ildefonse et al., 2007). The core is dominated by gabbroic lithologies and is moderately altered overall. The alteration of the core decreases and varies in style downhole. The alteration at times is linked to structural features such as faults and shear zones. High-strain crystal-plastic deformation is located in discrete shear zones that vary in thickness from millimeters to a few meters (see the “[Expedition 304/305 summary](#)” chapter).

This report presents the initial results of a pilot study utilizing the technique of electron backscatter diffraction (EBSD) to analyze the structural contrast between the center and the edge of a gab-

¹Halfpenny, A., and Prior, D., 2009. Data report: an electron backscatter diffraction study of a gabbroic shear zone, IODP Expedition 304/305. In Blackman, D.K., Ildefonse, B., John, B.E., Ohara, Y., Miller, D.J., MacLeod, C.J., and the Expedition 304/305 Scientists, *Proc. IODP, 304/305*: College Station, TX (Integrated Ocean Drilling Program Management International, Inc.).
doi:10.2204/iodp.proc.304305.201.2009

²Research School of Earth Sciences, Australian National University, Mills Road, ACT 0200, Australia. Correspondence author:
Angela.halfpenny@anu.edu.au



broic shear zone. Microstructures are studied with the overall aim of determining the controlling deformation mechanisms and the conditions of deformation within the shear zone. This work builds upon previous studies on oxide-rich shear zones performed by Agar and Lloyd (1997). The results of this study can be used to interpret whether these small shear zones have been involved in the uplift of the OCC or only represent minor phases of deformation inside the gabbro body during uplift and whether they are associated with late-stage injection of melts into the gabbroic body.

Methods and materials

Samples

Samples discussed in this data report were collected from Section 304-U1309D-64R-2 with the top of the billets at 43 and 46 cm from the top of the core (Fig. F1). This shear zone was chosen because of the clear contact between lithologies along the shear zone boundaries. It is located at 330 m depth (near the top of the total drilled core length) and is 8 cm wide. The bulk of Section 64R-2 is dunitic with a sheared gabbroic intrusion between 41 and 49 cm (although only the bottom contact was preserved in the core). The section exhibits mild greenschist facies alteration, and some chlorite is seen in the thin sections. Sample 64R-2, 43 cm, represents the center of the shear zone and is gabbroic in lithology (Fig. F2A, F2B). The bulk of thin section 64R-2, 43 cm, is plagioclase (~55%) and then clinopyroxene (~25%) with some orthopyroxene (~10%). There are minor amounts of opaques and alteration phases (talc, tremolite, and chlorite; ~10%). Sample 64R-2, 46 cm, exhibits both rock types and represents the edge of the shear zone and the lower contact with the dunite (Fig. F2D, F2E). The bulk of thin section 64R-2, 46 cm, is plagioclase (~50%) and then clinopyroxene (~20%) with some orthopyroxene (~10%) and hornblende (~10%). There are minor amounts of opaques and alteration phases (talc, tremolite, chlorite, and zeolite; ~10%).

Sample preparation

Samples were collected from the working half of the core once the shear zone of interest had been identified. The location for each of the thin section billets was chosen by studying the shear zone and choosing the best example of the microstructure exhibited by the sample. Thin section billets were oriented, where possible, with foliation perpendicular to either the long or short axis of the thin section billet, or the data were rotated subsequent to acquisition (Fig. F2C, F2F). Standard 30 μm thick thin sections were

produced from the billets. Thin sections were chemically and mechanically polished using SYTON fluid (Lloyd, 1987) and were carbon coated to prevent charging.

Data acquisition

Sample analysis areas were selected using optical and electron microscopy utilizing orientation contrast (OC) imaging (Prior et al., 1996). OC images show where crystallographic orientations change. Full crystallographic orientation data were obtained from automatically indexed EBSD patterns collected on a CamScan X500 Crystal Probe scanning electron microscope (SEM) fitted with a field emission gun and a FASTRACK stage (Prior et al., 1999). EBSD patterns were collected using a 20 kV acceleration voltage and a beam current of 30 nA. The working distance was 25 mm with an angle of 70° between the beam and the thin section. The step size of 3 μm was chosen as appropriate because of the size and details of the area to be mapped. Samples were mapped utilizing beam movement. EBSD patterns were imaged on a phosphor screen, viewed by a low-light charge-coupled device (CCD) camera, and indexed using the HKL Technology manufacturer's software package Channel 5 (Schmidt and Olesen, 1989). Average measuring time per point was 0.26 s. The raw data files exhibit indexing between 45% and 74% of the microstructure, leaving 26% to 55% as nonindexed (EBSD patterns with no solution). The nonindexed points correspond to grain boundaries, cracks, holes, and phases which were not mapped for various reasons. The raw data files were manipulated by removing wild spikes (1 pixel that is inconsistent with its surrounding 8 neighbors) and by performing a nearest neighbor extrapolation to fill in nonindexed points. All data manipulation was performed in comparison with the band contrast map to make sure that errors were not introduced. Grain sizes are calculated by the software from the manipulated EBSD maps (where grains <12 μm have been removed as they are considered errors) as the diameter of a circle of equivalent area to the measured grain area.

Results

Microstructural characteristics

The deformed grains of all phases are elongate parallel to the foliation, although the amount of elongation varies between each phase in both samples (Fig. F3). Sample 304-U1309D-64R-2, 43 cm, represents the center of the shear zone, and the grains of all phases are deformed but exhibit very few subgrain boundaries. The grain sizes of the phases except di-

opside are larger in Sample 64R-2, 43 cm (center of shear zone), than in Sample 64R-2, 46 cm (edge of shear zone) (Table T1). Sample 64R-2, 46 cm, shows a slightly better development of subgrain boundaries inside the plagioclase and hornblende, but the sample does not show much internal substructure overall. Most of the high-angle grain boundaries exhibit $\geq 30^\circ$ of misorientation across the boundary (black-colored boundaries).

Orientation data

Only orientation data for plagioclase is compared and presented in this section. Plagioclase was chosen for orientation analysis as it is the main mineral of the samples and is normally considered to be the weakest phase during deformation for a gabbro. Also, Sample 304-U1309D-64R-2, 43 cm, does not contain significant amounts of the other phases within the mapped area, so there is not enough data on the other phases to give a statistically viable crystallographic preferred orientation (CPO). The two samples show a similar CPO (Fig. F4). Sample 64R-2, 43 cm, from the center of the shear zone, exhibits a stronger texture than Sample 64R-2, 46 cm. In Sample 64R-2, 43 cm, *a*-axes form a distinct cluster 10° – 20° from the γ -direction, the *b*-axes are dispersed along a great circle on the lower hemisphere stereonet, and the *c*-axes are dispersed around the periphery of the upper hemisphere stereonet (Fig. F4A). In Sample 64R-2, 46 cm, *a*-axes form a distinct cluster 5° – 15° from the γ -direction, the *b*-axes are dispersed along a great circle on the lower hemisphere stereonet, and the *c*-axes are dispersed around the periphery of the stereonets (Fig. F4B).

Misorientation data

Statistically, the misorientation angle distribution (MAD) for plagioclase in both samples is dominated by a peak at 180° (Fig. F5A, F5B). An angle of 180° represents the rotation of the twin laws. A comparison between the neighbor-pair data and the theoretical random line shows that both plots also exhibit a small increase in the number of low-angle grain boundaries ($<10^\circ$). Both MAD neighbor-pair distributions exhibit a lull of relative frequencies of boundaries with misorientation angles in the range of 10° to 30° for Sample 304-U1309D-64R-2, 43 cm, and in the range of 15° to 35° for Sample 64R-2, 46 cm. The relative frequencies then increase after the lull to the peak at 180° (bimodal distribution).

Acknowledgments

The samples were obtained from IODP sample request number 20144B. Funding for the research was

provided by a National Environmental Research Council (NERC) IODP postcruise grant entitled “Deformation mechanisms, kinematics and conditions in an oceanic core complex: quantitative microstructural analysis of samples from IODP Expedition 305” (NERC grant code NE/D521549/1). I would like to thank Lorri Peters for editing the manuscript. I would also like to thank Geoffrey Lloyd, Elena Miranda, and Benoit Ildefonse for their useful scientific comments and suggestions, which helped to improve the manuscript.

References

- Agar, S.M., and Lloyd, G.E., 1997. Deformation of Fe-Ti oxides in gabbroic shear zones from the MARK area. *In* Karson, J.A., Cannat, M., Miller, D.J., and Elthon, D. (Eds.), *Proc. ODP, Sci. Results*, 153: College Station, TX (Ocean Drilling Program), 123–141. doi:10.2973/odp.proc.sr.153.009.1997
- Blackman, D.K., Cann, J.R., Janssen, B., and Smith, D.K., 1998. Origin of extensional core complexes: evidence from the Mid-Atlantic Ridge at Atlantis Fracture Zone. *J. Geophys. Res.*, 103(B9):21,315–21,334. doi:10.1029/98JB01756
- Blackman, D.K., Karson, J.A., Kelley, D.S., Cann, J.R., Früh-Green, G.L., Gee, J.S., Hurst, S.D., John, B.E. Morgan, J., Nooner, S.L., Ross, D.K., Schroeder, T.J., and Williams, E.A., 2002. Geology of the Atlantis Massif (Mid-Atlantic Ridge, 30°N): implications for the evolution of an ultramafic oceanic core complex. *Mar. Geophys. Res.*, 23(5–6):443–469. doi:10.1023/B:MARI.0000018232.14085.75
- Cannat, M., Sauter, D., Mendel, V., Ruellan, E., Okino, K., Escartin, J., Combier, V., and Baala, M., 2006. Modes of seafloor generation at a melt-poor ultraslow-spreading ridge. *Geology*, 34(7):605–608. doi:10.1130/G22486.1
- Ildefonse, B., Blackman, D.K., John, B.E., Ohara, Y., Miller, D.J., MacLeod, C.J., and Integrated Ocean Drilling Program Expeditions 304/305 Science Party, 2007. Oceanic core complexes and crustal accretion at slow-spreading ridges. *Geology*, 35(7):623–626. doi:10.1130/G23531A.1
- Lloyd, G.E., 1987. Atomic number and crystallographic contrast images with the SEM: a review of backscattered electron techniques. *Mineral. Mag.*, 51(359):3–19. doi:10.1180/minmag.1987.051.359.02
- Ohara, Y., Okino, K., and Kasahara, J., 2007. Seismic study on oceanic core complexes in the Parece Vela back-arc basin. *Isl. Arc*, 16(3):348–360. doi:10.1111/j.1440-1738.2007.00591.x
- Okino, K., Matsuda, K., Christie, D.M., Nogi, Y., and Koizumi, K.-I., 2004. Development of oceanic detachment and asymmetric spreading at the Australian-Antarctic Discordance. *Geochem., Geophys., Geosyst.*, 5(12):Q12012. doi:10.1029/2004GC000793
- Prior, D.J., Boyle, A.P., Brenker, F., Cheadle, M.C., Day, A., Lopez, G., Peruzzi, L., Potts, G., Reddy, S., Spiess, R., Timms, N.E., Trimby, P., Wheeler, J., and Zetterstrom, L., 1999. The application of electron backscatter diffraction

- and orientation contrast imaging in the SEM to textural problems in rocks. *Am. Mineral.*, 84(11–12):1741–1759.
- Prior, D.J., Trimby, P.W., Weber, U.D., and Dingley, D.J., 1996. Orientation contrast imaging of microstructures in rocks using foescatter detectors in the scanning electron microscope. *Mineral. Mag.*, 60(403):859–869. [doi:10.1180/minmag.1996.060.403.01](https://doi.org/10.1180/minmag.1996.060.403.01)
- Schmidt, N.-H., and Olesen, N.O., 1989. Computer-aided determination of crystal-lattice orientation from electron-channeling patterns in the SEM. *Can. Mineral.*, 27:15–22.
- Smith, D.K., Cann, J.R., and Escartin, J., 2006. Widespread active detachment faulting and core complex formation near 13°N on the Mid-Atlantic Ridge. *Nature (London, U. K.)*, 442(7101):440–443. [doi:10.1038/nature04950](https://doi.org/10.1038/nature04950)
- Tucholke, B.E., Lin, J., and Kleinrock, M.C., 1998. Megamullions and mullion structure defining oceanic metamorphic core complexes on the Mid-Atlantic Ridge. *J. Geophys. Res.*, 103(B5):9857–9866. [doi:10.1029/98JB00167](https://doi.org/10.1029/98JB00167)
- Initial receipt:** 3 February 2008
Acceptance: 25 July 2008
Publication: 30 January 2009
MS 304305-201

Figure F1. Photograph of hand specimen (Sample 304-U1309D-64R-2, 41–49 cm) from which thin section billets were cut. Red boxes = locations of thin sections, blue lines = locations of EBSD maps.

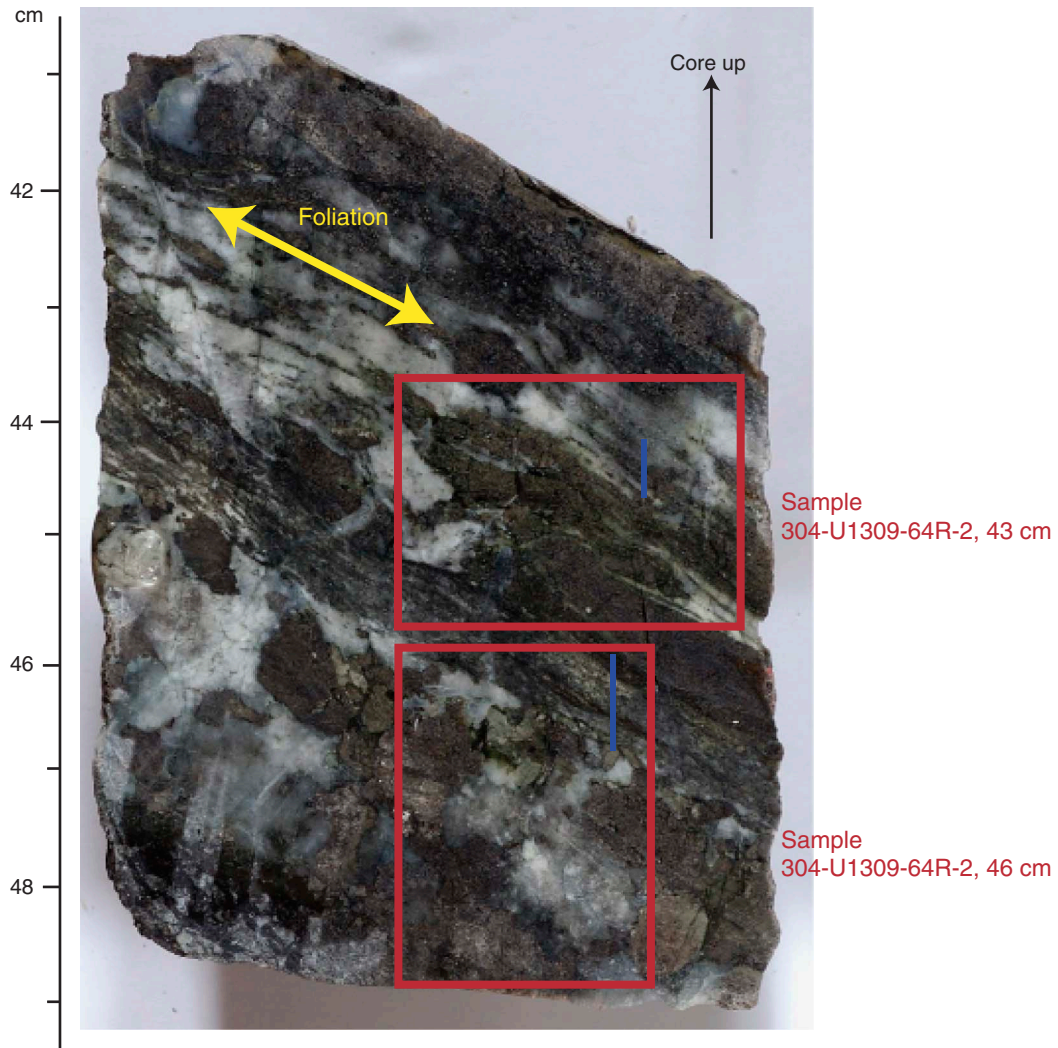


Figure F2. Samples 304-U1309-64R-2, 43 cm, and 64R-2, 46 cm. A, D. Plane-polarized light photomicrograph of full thin section. B, E. Cross-polarized light photomicrograph of full thin section. C, F. Stereonet summary marked with reference frames corresponding to thin section data acquisition. XZ reference frame = semikine-matic reference frame of thin section (foliation known but not lineation). XOYO reference frame = reference frame of maps produced by HKL Channel software. Northeast–southwest orientation of thin section foliation has been rotated to east–west in stereonet.

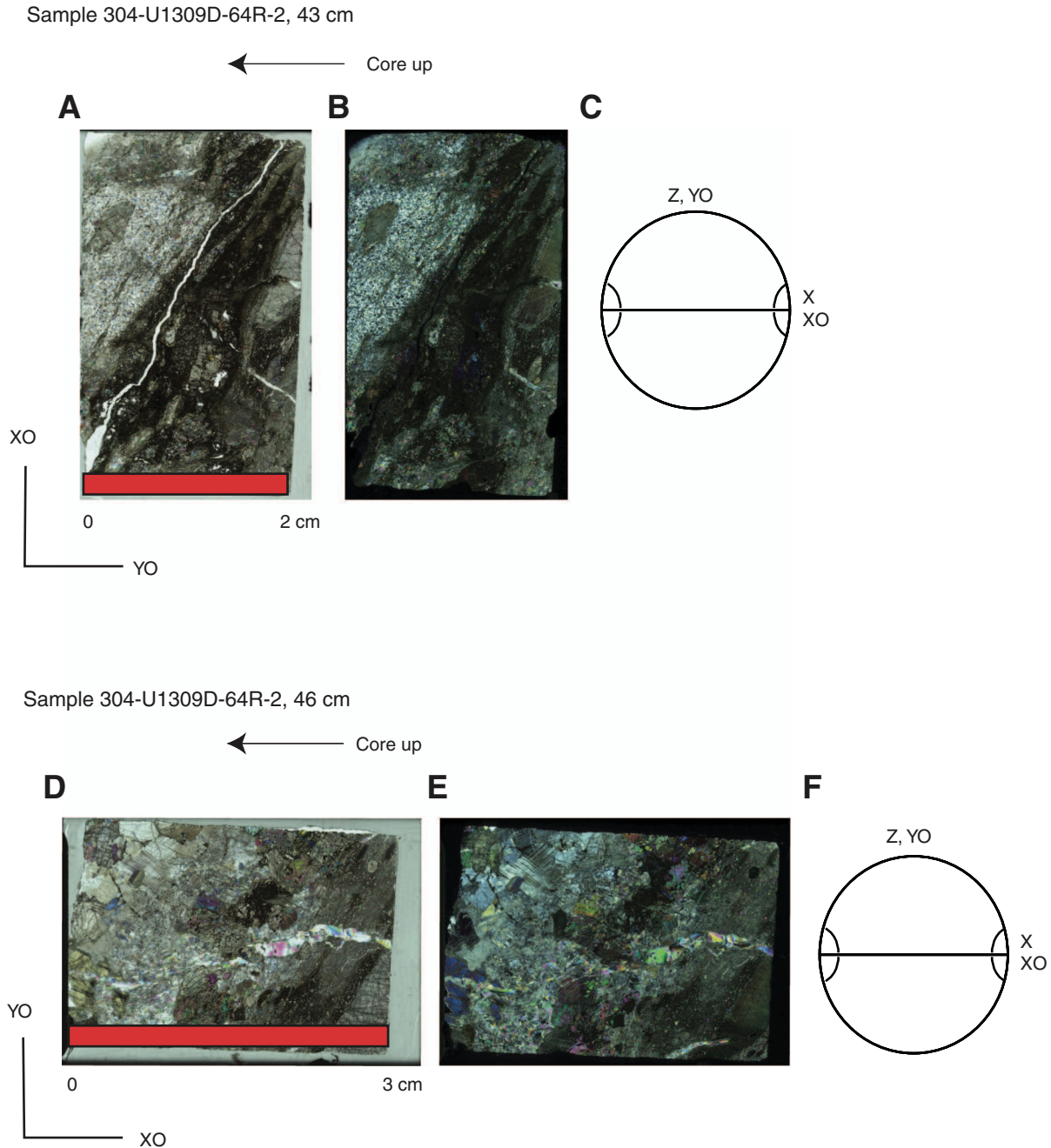


Figure F3. A, C. Band contrast (pattern quality) map for Samples 304-U1309D-64R-2, 43 cm, and 64R-2, 46 cm, with subgrain and grain boundaries marked (boundaries colored by misorientation angle between the two grains). Yellow $\geq 2^\circ$, lime green $\geq 5^\circ$, blue $\geq 10^\circ$, pink $\geq 20^\circ$, and black $\geq 30^\circ$. Boundaries between phases are marked in red. B, D. Phase map showing each mapped phase in a different color for Samples 304-U1309D-64R-2, 43 cm, and 64R-2, 46 cm, with grain boundaries marked. Blue = plagioclase, red = diopside, purple = enstatite, green = hornblende, yellow = ilmenite.

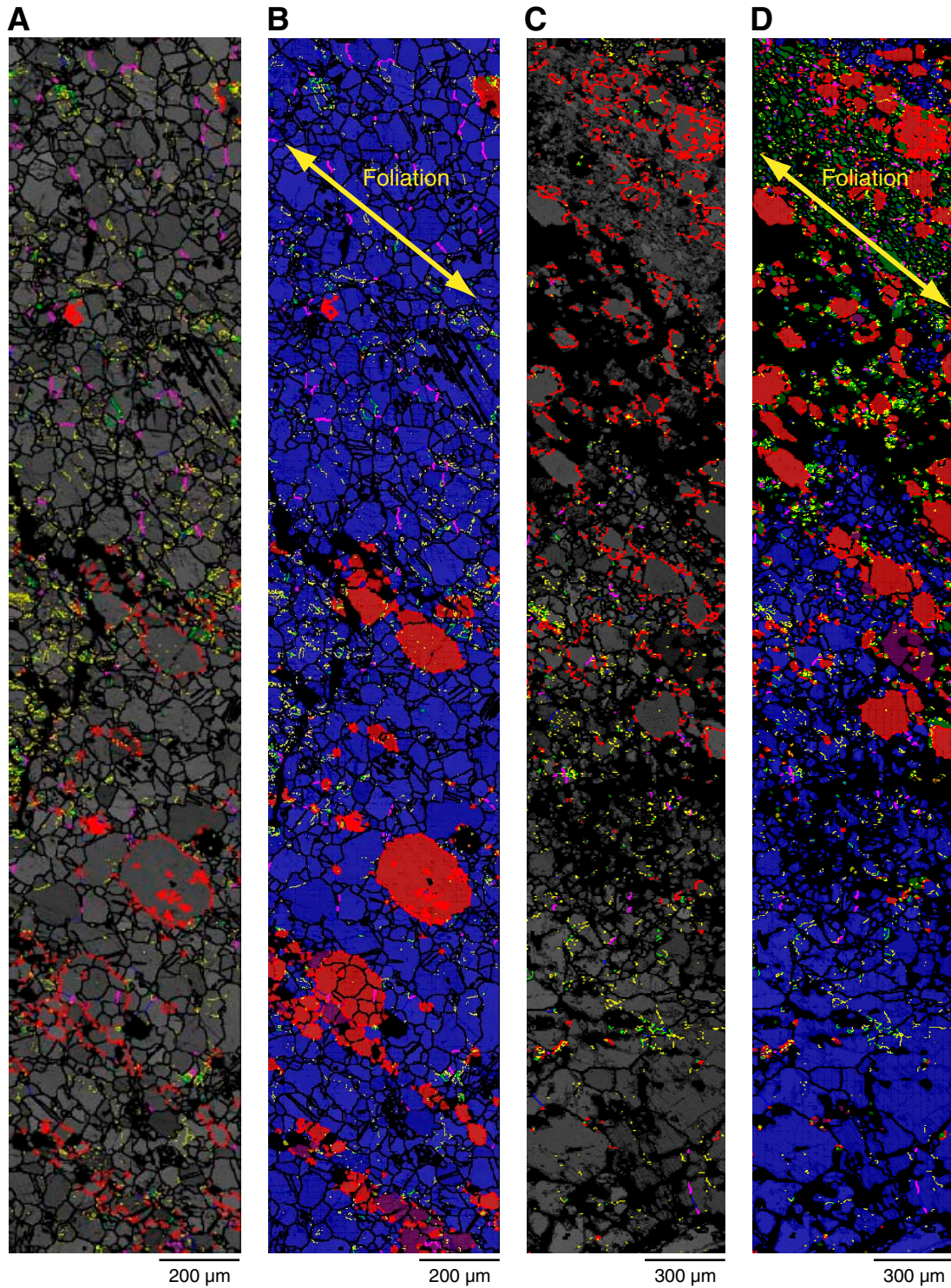


Figure F4. Equal area lower and upper hemisphere contoured stereonet for plagioclase CPO (counting cone half-width = 15°). **A.** Sample 304-U1309D-64R-2, 43 cm. **B.** Sample 304-U1309D-64R-2, 46 cm. One point per grain (ensures a false CPO is not shown because of the oversampling of one large grain). First stereonet shows kinematic framework where foliation is east–west perpendicular to the page (Z = pole to foliation).

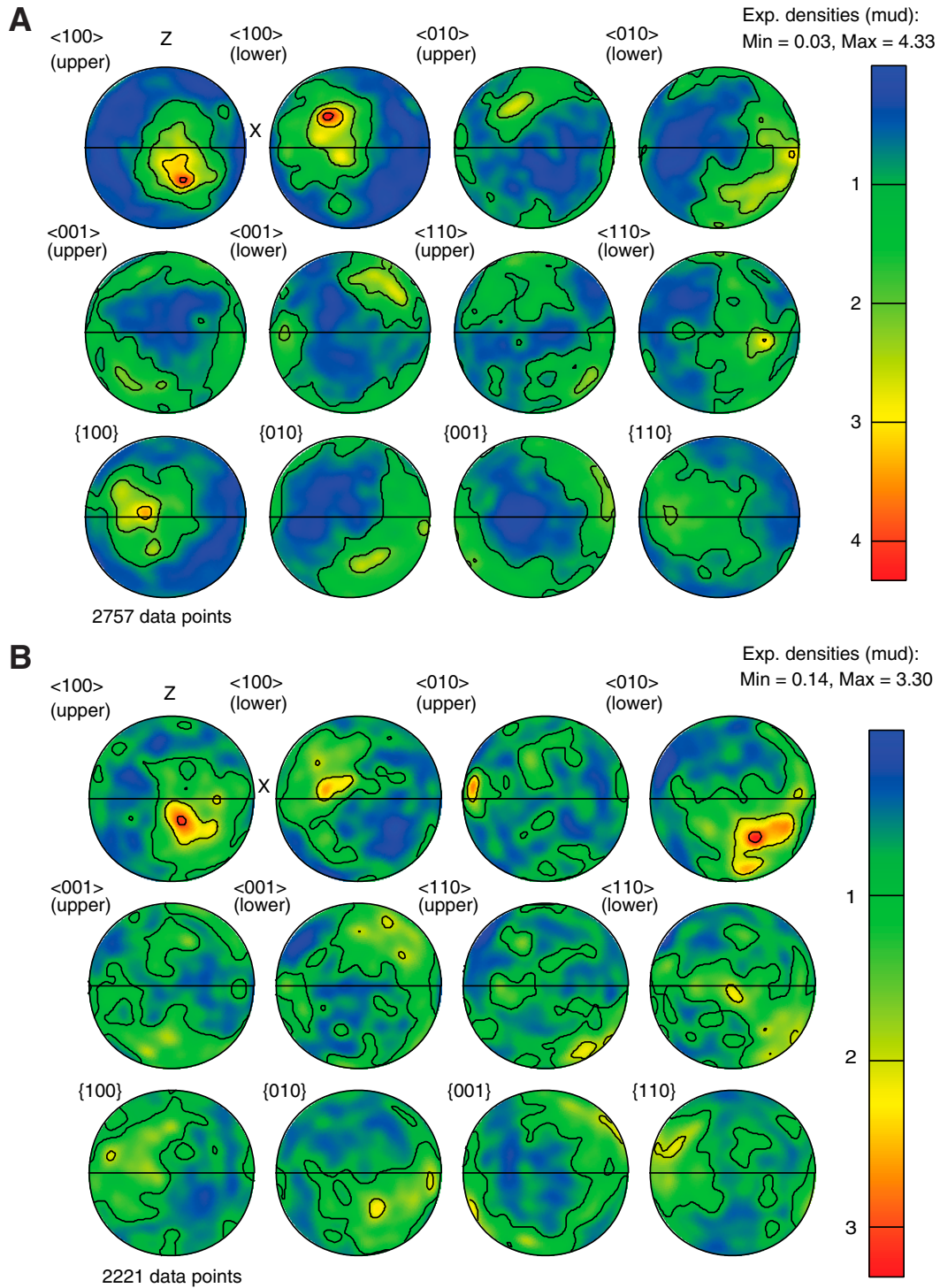


Figure F5. Misorientation angle distributions of plagioclase for Samples 304-U1309D-64R-2, 43 cm, and 64R-2, 46 cm, are plotted as frequency histograms for neighbor pairs and random pairs. Black smoothed line = theoretical random distribution. Sample 64R-2, 43 cm: random pairs = 1,000 data points, neighbor pairs = 117,512 data points. Sample 64R-2, 46 cm: random pairs = 1,000 data points, neighbor pairs = 27,882 data points.

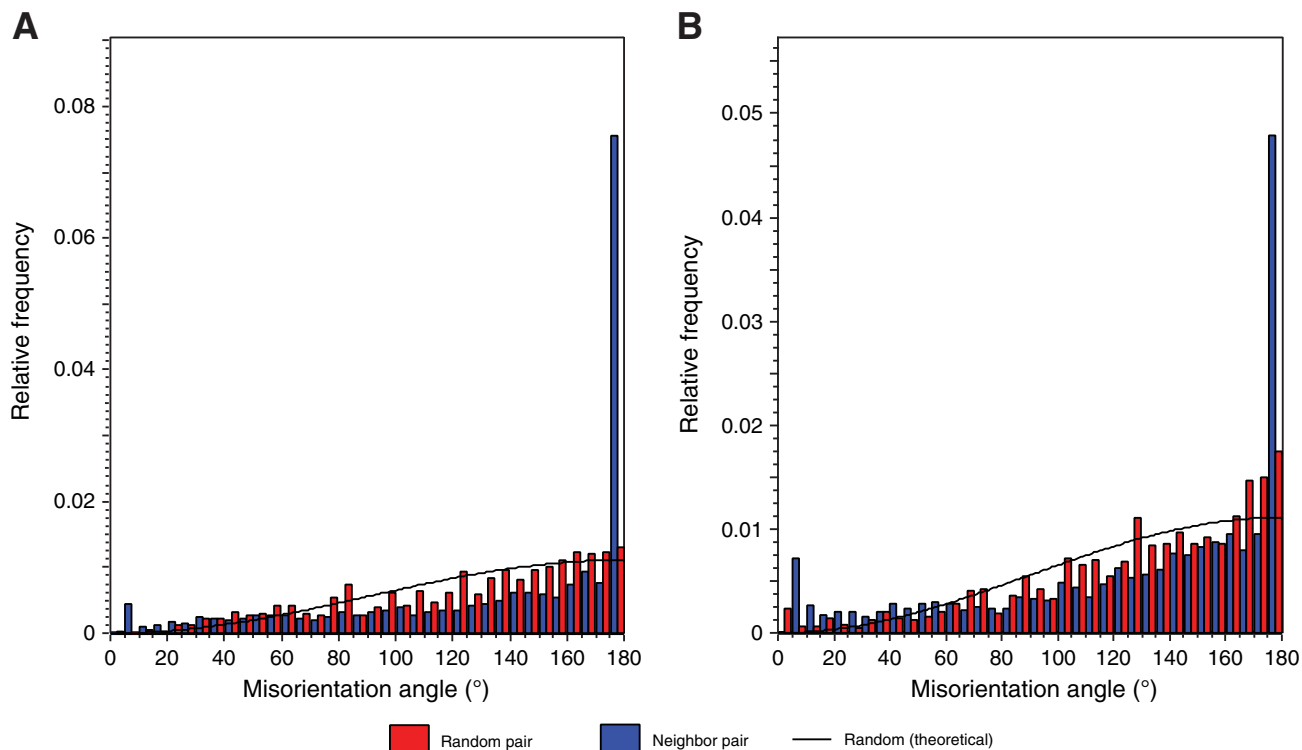


Table T1. Summary of grain-size statistics calculated from EBSD data. (See table notes.)

Phase	Mean (μm)	Standard deviation (μm)	Median (μm)
Center of shear zone:			
Plagioclase	45.5	35.7	34.2
Enstatite	33.3	28.1	22.5
Diopside	43.9	40.7	34.4
Ilmenite	18.4	6.1	16.2
Edge of shear zone:			
Plagioclase	26.7	24.2	20.3
Enstatite	24.8	19.1	19.7
Diopside	35.7	29.9	26.4
Ilmenite	15.5	2.9	14.8
Hornblende	21.5	8.0	19.4

Notes: Grains are defined as domains surrounded by boundaries with 10° or more misorientation. Grains $<12 \mu\text{m}$ have been removed from the analysis, as most errors created during the data collection, noise reduction, and data manipulation phases show up as small grains. Center of shear zone data from Sample 304-U1309D-64R-2, 43 cm; edge of shear zone data from Sample 64R-2, 46 cm.